CrossMark

Anodic Electrophoretic Deposition of Graphene Oxide on 316L Stainless Steel with pH-Dependent Microstructures

Geetisubhra Jena[1,2] · S. C. Vanithakumari[1] · C. Thinaharan[1] · R. P. George[1] · U. Kamachi Mudali[2,3]

Abstract

This paper describes anodic electrophoretic deposition of graphene oxide (GO) on 316L SS with pH-dependent microstructures. GO flakes were synthesized by modified Hummers' method. Detailed studies on structural characteristics, thermal stability, and elemental composition of the GO flakes were carried out using advanced characterization techniques. Results showed successful oxidation and exfoliation forming GO flakes that are hydrophilic in nature. Acidic (pH 3.4) and basic (pH 11) aqueous GO suspensions were prepared, and the zeta potential as well as the average particle size distribution of the suspensions was ascertained. The GO suspensions were exhibiting zeta potential values of −32.9 and −36.8 mV and average particle size of 1–2 μm and 800–900 nm at acidic pH of 3.4 and alkaline pH of 11, respectively. Using anodic electrophoretic deposition (EPD) methods, GO was coated on 316L SS substrate from acidic and alkaline suspension and coatings were characterized. The increased value of I_D/I_G by Raman spectra analysis, partial restoration of C=C skeleton in the de-convoluted C 1s XPS spectra analysis, and the presence of C–C and C–H stretching bands in ATR-FTIR spectra were correlated with partial reduction of GO during the deposition on 316L SS surface. Though there was no difference in the chemical composition of the coatings formed from the acidic and alkaline pH suspension, atomic force microscopy and field emission scanning electron microscopy characterization showed difference in topography and morphology of the coatings. 316L SS substrates coated with GO in acidic pH showed higher RMS and average roughness and dense agglomerated wrinkled microstructure compared to substrates coated with alkaline pH suspension. Again GO coating from acidic pH suspension showed hydrophobicity. The present study showed that the microstructures of the GO coatings on 316L SS can be tuned by varying the pH of the GO suspension during EPD process.

Graphical Abstract

Alkaline pH -11 (pH of GO suspension adjusted by NaOH)

85.3±1.6°

Acidic pH- 3.4 (As prepared GO suspension)

91.2±2.3°
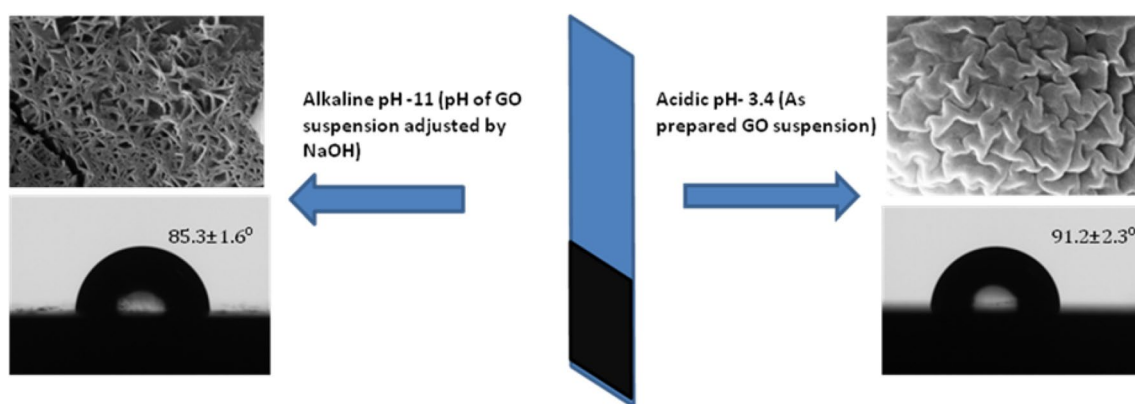
Keywords Graphene oxide · Electrophoretic deposition (EPD) · pH · Zeta potential · Microstructure · Contact angle

Extended author information available on the last page of the article

1 Introduction

Applications of the novel graphene-based materials emphasize the synthesis and fabrication of graphene oxide on different substrates by simple and cost-effective methods. Graphene refers to the family of graphitic materials, including pristine graphene (G), graphene oxide (GO), and reduced graphene oxide (rGO) [1]. Graphene exhibits a flat (2D), single-layer tightly packed honeycomb structure with sp^2-bonded carbon atoms, which is the basic block for all other structured graphitic materials [2]. Wang et al. [3] reported the synthesis of large-scale and highly efficient graphene by electrolytic exfoliation method. The solvothermal and sonication-assisted graphene production was reported by Choucair et al. [4]. Wang et al. [5] produced graphene nanosheets in large quantity via synthetic chemical route involving oxidation of natural graphite, followed by ultrasonic exfoliation, and chemical reduction. Graphene oxide sheets are the oxygen-functionalized derivatives of graphene, consisting of monolayer carbon atoms with oxygen-containing functional moieties. The widely accepted structural model for GO was proposed by Lerf and Klinowski [6]. Basically, graphene basal plane consists of hydroxyl and epoxy groups, and the edges of the sheets are occupied by carboxyl moieties. Because of these oxygen-containing groups, defects are introduced into the graphite stacked sheets. These oxygen functional groups in graphene sheets impart hydrophilicity to the individual sheets. As reported by Konkena and Vasudevan [7], the pH changes brought in by the addition of acids and bases reveal the key role of the carboxyl groups in the suspension characteristics. The GO is considered as an insulator because of the distortion of sp^2-hybridized graphene structure [8]. Nevertheless, the graphitic distortion-less structure can be restored by reducing the oxygen functional group either by chemical reductants or by heat treatment [9].The hydrophilicity of GO also opened a new channel to synthesize many composite materials which find wide applications as antimicrobial coatings [10–12], corrosion-resistant coatings [13], in microelectronics [14], etc.

For the fabrication of graphene derivatives on conductive and nonconductive substrates, coating techniques such as chemical vapor deposition (CVD) [15, 16], Langmuir–Blodgett method [17, 18], and electrophoretic deposition (EPD) [13, 19–22] have been employed. Among these techniques, EPD is proven to be the most effective method with respect to simple instrumentation, economic viability, and ease of coating of graphene derivatives on conductive substrates. The increasing interest toward EPD technique is also due to the formation of a uniform, stable, and few nanometer-thick coating [21]. Another advantage of EPD is that there is no constraint on substrate dimensions. Diba et al. [22] studied the EPD kinetics of GO on indium tin oxide (ITO) substrates by varying the deposition time and voltage. Flexible reduced GO membrane on stainless steel substrate was developed using EPD method by Wang et al. [23]. The EPD method was adopted by Sung et al. [20] to fabricate GO platelets on 200 mesh stainless steel. Deposition of GO on mild carbon steel by EPD was carried out by Park et al. [24]. Singh et al. [13] reported the deposition of GO composite on Cu substrate by EPD. The stability of GO colloid in water medium depends on the ionization of carboxyl group as well as electrostatic repulsion among the negatively charged carboxylate ions and is crucial for EPD process. Apart from these physical restrictions, the well-established mathematical model for the EPD kinetics proposed by Hamaker [25] predicts that the deposited mass during EPD process is directly proportional to the deposition time, concentration of the loaded particles, electric field strength, and surface area of the electrodes used as well as the electrophoretic mobility which is correlated with zeta potential.

Due to excellent corrosion resistance offered by passivation, stainless steels are used in aggressive corrosive environments [26–29]. However, there is a big concern that stainless steels are susceptible to localized corrosion in chloride environments. Therefore, in the present study, an attempt has been made to deposit GO on 316L SS using EPD for developing a corrosion-resistant coating for chloride environments. Successful synthesis of GO flakes by modified Hummers' method, and anodic electrophoretic deposition of graphene oxide on 316L stainless steel with pH-dependent microstructures, is described in this paper.

2 Experimental Methods

2.1 Materials

Graphite powder with a purity of 90% from Nice was used to prepare GO. Type 316L austenitic grade stainless steel (Fe, < 0.03% C, 16-18.5% Cr, 10-14% Ni, 2-3% Mo, < 2% Mn, < 1% Si, < 0.045% P and < 0.03% S) coupons of dimensions $35 \times 25 \times 3$ mm were polished with silicon carbide grit sheets up to 1000 grit. The polished samples were washed with Millipore water and acetone successively for 10 min using a bath sonicator and were employed as both working and counter electrodes in the EPD.

2.2 Synthesis of GO Flakes

Graphene oxide was prepared by modified Hummers' method through oxidation of as-received graphite powder [30, 31].About 1 g of graphite and 1 g of $NaNO_3$ were taken in a beaker and kept in an ice bath. 50 ml of H_2SO_4 was

introduced into the beaker containing the reaction mixture. The solution was stirred for 30 min, and 7 g of $KMnO_4$ was added to the acid mixture slowly, over an hour. The solution was stirred continuously for complete dissolution of $KMnO_4$. The temperature of the homogeneous mixture in the beaker was raised to 35 °C, and stirring was continued for 2 h. The mixture was cooled to room temperature and then added to ~ 90 ml of Millipore water slowly. About 3 ml of 30% H_2O_2 was added subsequently for reducing the residual permanganate and manganese dioxide to water-soluble manganese sulfate. Addition of 30% H_2O_2 is considered as the purification step during GO preparation. Another 55 ml of Millipore water was further added for washing the GO. The bright yellow-colored reaction mixture was kept undisturbed to allow the GO to settle down, and the supernatant was discarded. The GO was washed with 3% HCl (100 ml) to remove the metal ions from the solution. This was followed by washing with Millipore water several times till neutral pH was achieved. Then, after washing with ethanol twice, the GO prepared was kept in an oven at 60 °C for drying. From 1 g of graphite, 1.496 g of GO was synthesized using modified Hummers' method.

2.3 Characterization of GO Flakes

Elemental analysis (Carbon/Hydrogen/Nitrogen/Sulfur) was carried out using CHNS system (Elementar, Model: Vario MICRO cube) by a conventional combustion method, based on the burn off of the sample, and the gases were detected by a thermo-conductivity detector (TCD) to obtain the weight percentage of elements present in the GO flakes. Fourier transform infrared (FTIR) spectra were recorded using infrared spectrometer (ABB, Versatile FTIR Laboratory Spectrometer, Model: MB3000, Canada) in the range 400–4000 cm^{-1}. X-ray diffraction (XRD) pattern was recorded by X-ray diffractometer (Inel X-Ray Diffractometer, 35 kV, 20 mA Equinox 2000, France) using Co K_α radiation ($\lambda = 1.79$ A°) in the 2θ range 0°–80°. Thermogravimetric analysis (TGA) was carried out using the Calorimetry and Thermal Analysis Unit (SETSYS 12, Setaram, France) in the temperature range 25–800 °C with the heating rate of 5 °C/min and with argon gas purging. For TGA, 4 mg of GO flakes was used. Proton-decoupled ^{13}C NMR was recorded with Bruker Avance IIIHD spectrometer, in a magnetic field of 9.4 T and the resonance frequency of ^{13}C as 100.64 MHz in order to identify the different carbon environments existing in the prepared GO flakes in the range 0–180 ppm (parts per million) on TMS (Tetramethylsilane) scale. The Raman spectrum and AFM topography of the GO flakes were recorded using Multiview 2000 instrument (Nanonics, Israel) coupled with Olympus optical microscope, using a 50X objective lens employed for both, excitation and collection. Nd: YAG laser having a wavelength of 532 nm was

used as the excitation source. The laser power on the sample's surface was 3 mW. The laser spot size of 0.7 μm diameter was focused on the sample surface using diffraction-limited 50X objectives. The Raman spectrum was acquired over the range 1000–1700 cm^{-1} with 1 s exposure time and 50 CCD accumulations. Field emission scanning electron microscope (FESEM) image of the GO flakes was taken using Gemini, Zeiss, Germany. For SEM investigation, the GO suspension was drop coated over sapphire substrate. The analysis of oxygen-containing group in GO flakes was carried out using X-ray photoelectron spectroscopy (XPS) (SPECS, Germany) system equipped with a monochromatic Al Kα source (1486.7 eV) operated at 350 W with detection pass energy of 10 eV. The high-resolution spectra of carbon and oxygen were acquired for all the samples and fitted with Gaussian–Lorentzian line shapes using CASA XPS software. The assignment of C 1s and O 1s components was based on the data available in literature.

2.4 Preparation of GO Suspension

GO flakes of concentration 1 mg/ml were dispersed in the suspension medium (Millipore water with a conductivity of 0.5 μS/cm) by ultrasonication (Ultrasonic Processor, Hielscher, UP400S) for 1 h at room temperature. The pH of the GO suspension was varied from acidic to alkaline using 2M NaOH solution.

2.5 Characterization of the GO Suspension

Zeta potentials and average particle size distribution of the as-prepared GO suspension and pH-varied GO suspensions were measured using dispersion optical analyzer (Zeta sizer, Malvern, ZEN3690) to establish the stability of the suspension. Absorbance of the aqueous suspension of GO flakes was measured using UV–Vis spectrophotometer (Shimadzu, UV-2450) in the range 900-200 nm.

2.6 Anodic Electrophoretic Deposition of GO on 316L SS

The EPD was carried out using two GO suspensions with pH 3.4 (acidic) and pH 11 (alkaline). The 316L SS coupons served as both working electrode (anode) and counter electrode (cathode) in the EPD process [19, 20]. The two electrodes were immersed in as-prepared GO suspension. The distance between working electrode and counter electrode was kept constant as 10 mm during EPD process, and the electrodes were connected to a regulated DC power supply (AplabTS3202D). Other parameters such as deposition time, concentrations of GO, and applied voltage were kept constant. After EPD process, the coated samples were dried

in ambient conditions. Schematic of GO coating on 316L SS by EPD is shown in Fig. 1.

2.7 Characterization of GO-Coated 316L SS

The Raman spectra and AFM topography of the GO-coated substrates were recorded using Multiview 2000 instrument. Attenuated total reflectance Fourier transform infrared (ATR-FTIR) transmission spectra were recorded for 316L SS substrates coated with GO suspension of pH 3.4 and pH 11 using infrared spectrometer (Bruker, Germany) in the range 500–4000 cm^{-1}. The surface morphologies were investigated using FESEM (Gemini, Zeiss Germany). Water contact angles (WCA) for GO-coated samples were measured using the contact angle goniometer (OCA15EC, Data Physics Instruments, Germany). The WCA measurements were recorded at five different locations using sessile drop method using Millipore water of 10 µl dosing volume with a dosing rate of ~ 1 µl s^{-1}, and their average was taken as the WCA of the coated substrates. XPS characterization of 316L SS substrates coated with GO suspension of pH 3.4 and pH 11 was carried out with same instrumental parameters as given in 2.3 for GO flakes.

3 Results and Discussion

3.1 Characterization of Synthesized GO Flakes

The result of the elemental analysis of GO powder is given in Table 1. The weight percentage of C in GO sheet was about 39.48%. In addition, H (3.39%) and S (1.69%) were observed

Table 1 Elemental analysis of GO flakes

Element (in %)	Carbon	Hydrogen	Sulfur	Oxygen
GO	39.48	3.39	1.69	55.44

in the GO flakes. The content of O in GO was about 55.44%. Functional groups analysis of the as-prepared GO flakes using FTIR spectroscopy showed a strong and broad peak between 2800 and 3700 cm^{-1} and a sharp peak at 1402 cm^{-1} in the spectrum reproduced in Fig. 2a, corresponding to the stretching and bending vibrations of the O–H groups of carboxylic acid present on the edges of GO sheets as well as water adsorbed on GO, respectively. C–H vibrational stretching band is observed at ~ 2360 cm^{-1} and assigned to either symmetrical or asymmetrical > CH_2 bonds. Two absorption peaks observed at 1627 and 1735 cm^{-1} could be attributed to the stretching vibration of C=C and C=O of carboxylic acid and carbonyl groups present at the edges of GO. The absorption peaks at 1229 and 1087 cm^{-1} corresponded to the stretching vibration of C–O of epoxy and C–OH of alcohol, respectively. The presence of these oxygen-containing groups revealed that graphite had undergone oxidation and the synthesized product was hydrophilic in nature due to its tendency to form hydrogen bonds with water [31]. The oxidation of graphite was further characterized by XRD. XRD technique is very sensitive to interplanar crystal structure as well as the distortion occurring in layer structures. XRD pattern (Fig. 2b) of natural graphite showed one intense and sharp peak at 2θ value of 30.65° corresponding to the (002) plane, and a low intense peak was observed at 51.5° corresponding to the (004) plane. For GO flakes, a broad peak
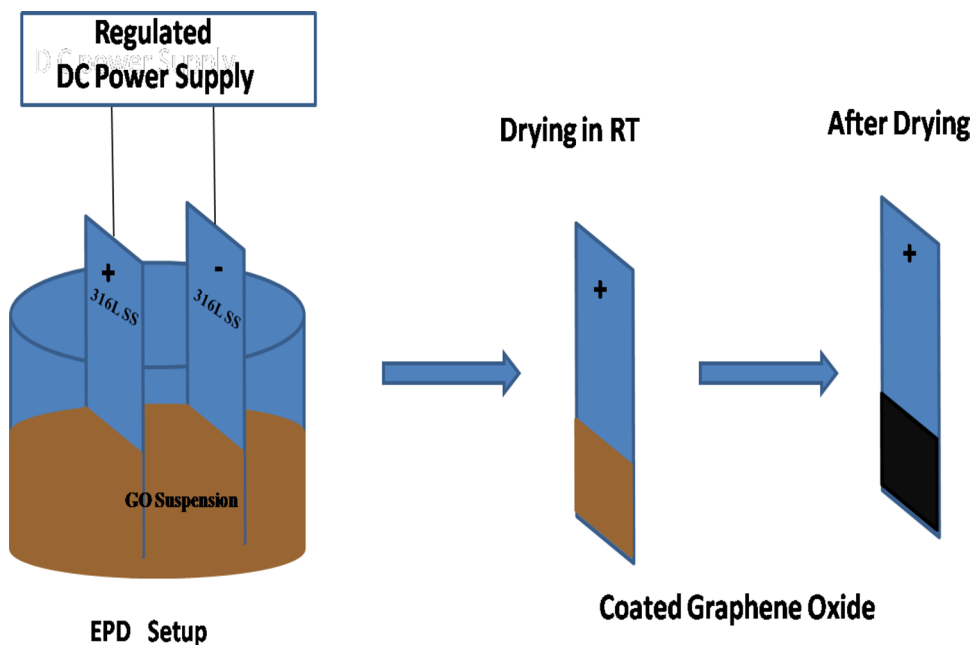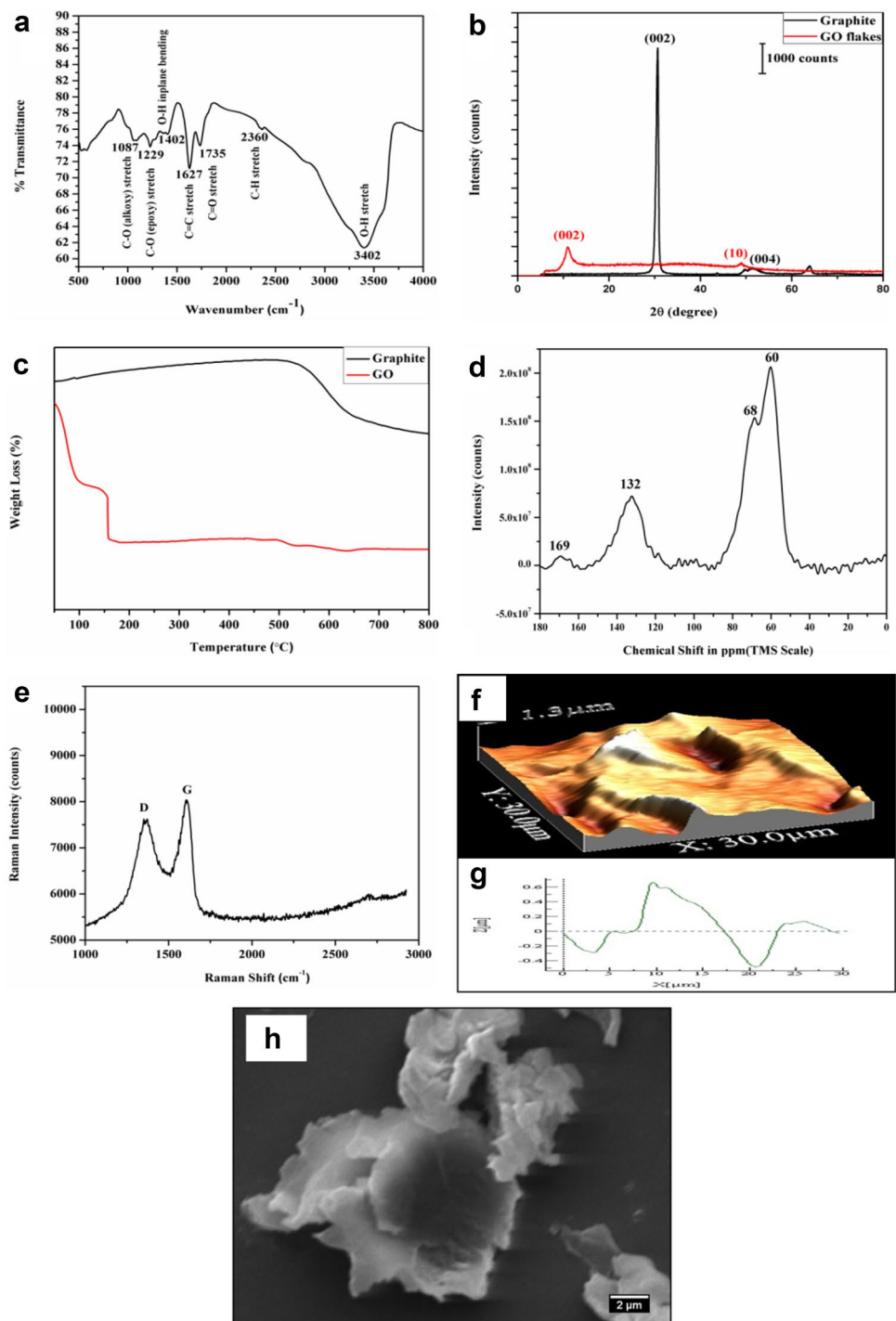

Fig. 1 EPD setup for GO coating on 316L SS

Fig. 2 **a** FTIR transmission spectrum, **b** XRD spectrum, **c** TGA curve, **d** ^{13}C NMR spectrum, **e** Raman spectrum, **f** AFM image, **g** height profile, and **h** scanning electron micrograph image of GO flakes produced by modified Hummers' method

was observed at 2θ value of 10.87° corresponding to the (002) reflection, indicating the interplanar distance between the graphene layers. The FWHM of (002) reflection in GO flakes was broader and peak intensity was lower than natural graphite. The shift was also observed in (002) reflection in GO flakes implicating the presence of strains/defects as well as larger interplanar *d* spacing. Another peak at 2θ value of 48.97° in GO flakes corresponding to the plane

(10) indicates the short range order of stacked graphene oxide layers [32]. Applying the Bragg's law to the reflection (002), the interplanar distance was evaluated to be 0.33 and 1.79 nm for natural graphite and GO flakes, respectively. The larger interplanar spacing indicated the successful oxidation of graphite by modified Hummers' method. The Scherrer equation was applied to the reflection (002) by taking structural factor value as 0.9, and the average height of natural

graphite and graphene oxide stacking layers was calculated to be 15.198 and 5.492 nm, respectively. The decrease in average height of stacking layers indicated the successful chemical exfoliation that has occurred during the oxidation of natural graphite to GO flakes. The Scherrer equation was also applied to the two-dimensional reflection (10) using the value of Warren constant as 1.84 [33], and the average diameter of stacking layers was estimated to be 24.97 nm. Figure 2c shows the results of the thermogravimetric analysis of GO flakes. From the figure, it is evident that the weight loss in natural graphite was in one step in the temperature range 465–731 °C, while GO decomposed in three steps. The first weight loss in GO at 27–126 °C corresponded to the loss of water molecules. The second step weight loss observed in the range 127–225 °C is due to the decomposition of oxygen-containing groups, and the third step weight loss above 500 °C is pertained to the combustion of graphene structure. The report by Sasha et al. [34] corroborated this observation. In concordance with the literature data [35], the proton-decoupled ^{13}C NMR spectrum of GO flakes (Fig. 2d) consisted of four peaks at 60, 68, 132, and 169 ppm (parts per million). The first two peaks (60 and 68 ppm) are known to originate from tertiary C–OH and C–O–C groups, respectively [35]. In the present study, the C–OH and C–O–C group peaks were not prominent. Rather, they appeared to be merged, because of the condensation of C–OH groups to form C–O–C linkage. The third peak around 132 ppm showed the presence of very stable aromatic C=C regime. The less intense peak corresponding to the C=O peak from carboxylic acid group at 169 ppm was present at the edges of the GO sheet.

Raman spectroscopy, which is a nondestructive technique, was used for the characterization of carbon products to provide information regarding degree of hybridization, crystal disorder, the extent of chemical modification, and distinction of single-layer graphene structure to multilayer graphene structure. The Raman spectra arising from the lattice vibrations (phonons) of graphitic materials consisting of stacked graphene layers are very sensitive to the degree of structural disorder (defects). The Raman spectrum for GO flakes is shown in Fig. 2e. It revealed a D band around 1359.7 cm^{-1} and a G band around 1607.08 cm^{-1} with I_D/I_G value as 0.94. The G mode is a doubly degenerated phonon mode of in-plane E_{2g} symmetry at Brillouin zone center originated from in-plane vibration of C=C conjugate bonds. The D mode is arising from the doubly resonant disorder-induced mode of graphitic hexagonal structure [19, 34]. Figure 2f, g shows the AFM topography of GO flakes with its height profile. Topography showed the well-defined sharp edges of GO sheets present in prepared GO flakes. The height profile showed the average roughness and RMS roughness of GO flakes as 155.7 and 200.0 nm, respectively. The FESEM analysis indicated the morphology of the GO

flakes to be crumbled paper sheets with sharp edges and multiple-layered-like structure, as shown in Fig. 2h. XPS is widely being used to analyze oxygen-functionalized graphitic material as well as its coating on various substrates. Since GO is synthesized by the oxidation of graphite, it is found from many characterization techniques that oxygen-containing groups exist in the forms of hydroxyl, carbonyl, and epoxide attached to the graphene basal plane [36]. The de-convoluted C 1s and O 1s spectra of GO flakes are presented in Fig. 3a, b. The C 1s spectrum of GO flakes showed the binding energy at 284.8, 285.7, 286.8, 287.9, and 289.5 eV was assigned to C=C (sp^2-bonded graphene basal plane skeleton), C–OH, C–O–C, > C=O, and O=C–OH, respectively, present in GO flakes. The lowest intense peak for C=C corresponded to the successful oxidation of graphite. The quantification result of de-convoluted C1s spectrum showed the atomic percentage of carbon as 3% in C=C regime. The O1 s spectrum of GO can be curve-fitted into five peaks, which are corresponding to HO-C=O (carboxyl 531.4 eV), > C=O (carbonyl 532 eV), C–O–C (epoxy 532.6 eV), C–OH (hydroxyl 533.4 eV), and adsorbate like water or hydrate (534 eV), respectively. The assignments are in agreement with the literature [36–38]. No metal oxide peak was observed in GO flakes.

3.2 Characterization of GO Suspension

The zeta potentials measured for the GO suspensions at different pH are plotted in Fig. 4a. The GO suspensions were exhibiting zeta potential values of −32.9 and −36.8 mV at an acidic pH of 3.4 and alkaline pH of 11, respectively. The negative zeta potential values are due to the presence of electronegative functional groups formed on the graphene sheets during oxidation. With the successive increase in oxidation, more number of electronegative functional groups are formed in GO resulting in high negative zeta potential values [39]. The stability of GO suspension is improved by adding NaOH because it acted as a hydrogenating agent for graphene oxide. It has the ability to remove oxygen functional groups from GO sheets and make it as activated graphene sheets. The change in color to black and stability could be due to the decrease in particle size and well-dispersed suspension. For the GO suspension with acidic pH 3.4, the average particle size varied in the range of 1–2 μm. The average particle size varied in the range of 800–900 nm for the GO suspension with alkaline pH 11. Two characteristic peaks were observed in the UV–Vis spectrum (Fig. 4b) of the aqueous dispersion of GO [40], recorded over the range of 200-900 nm. The intense absorption peak observed at 232.5 nm corresponded to a π–π* plasmon transition. Appearance of π–π* plasmon transition is due to two kinds of conjugation effects. One of these conjugation effects is associated with sp^2 planar cluster, and the other one is
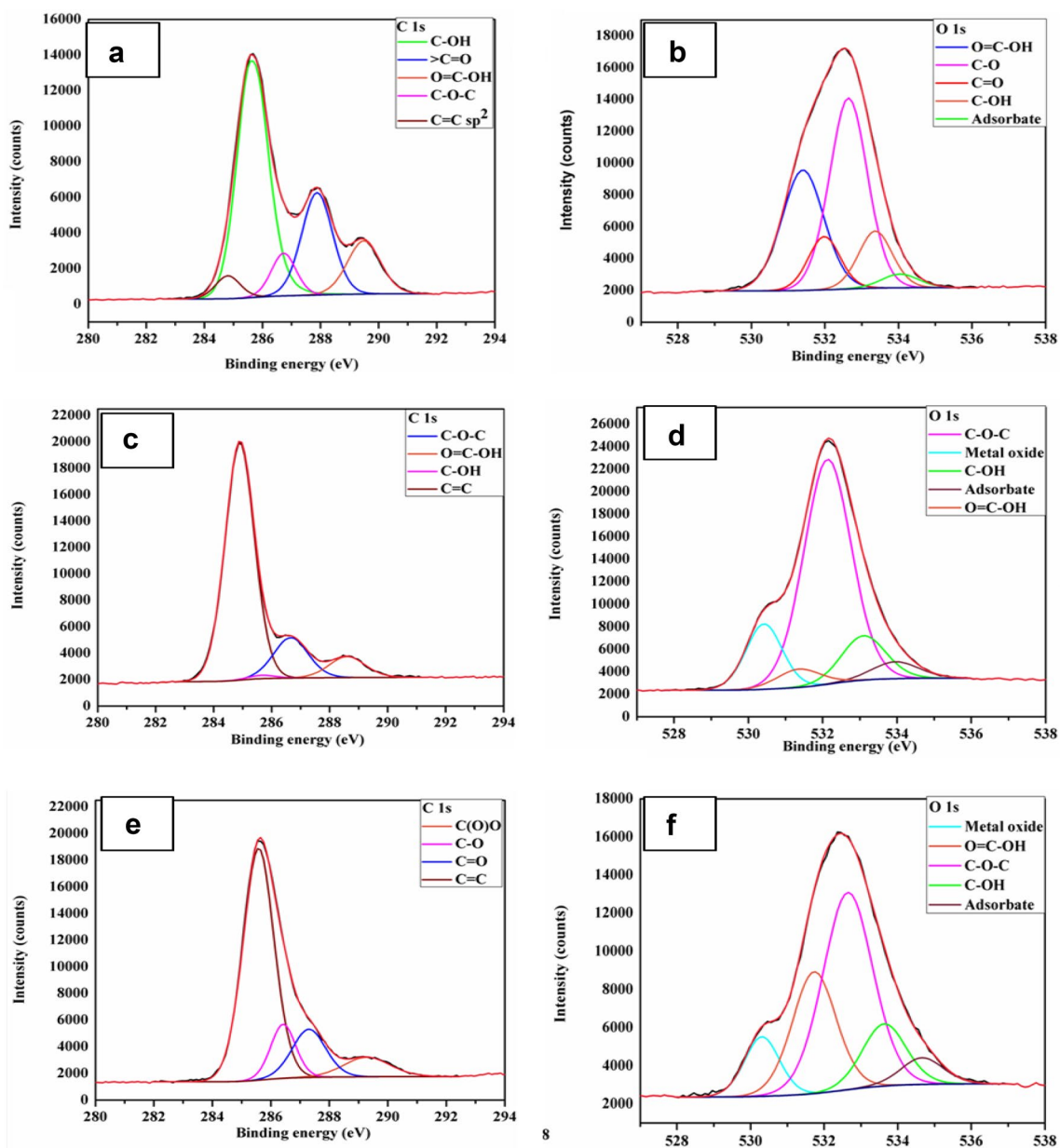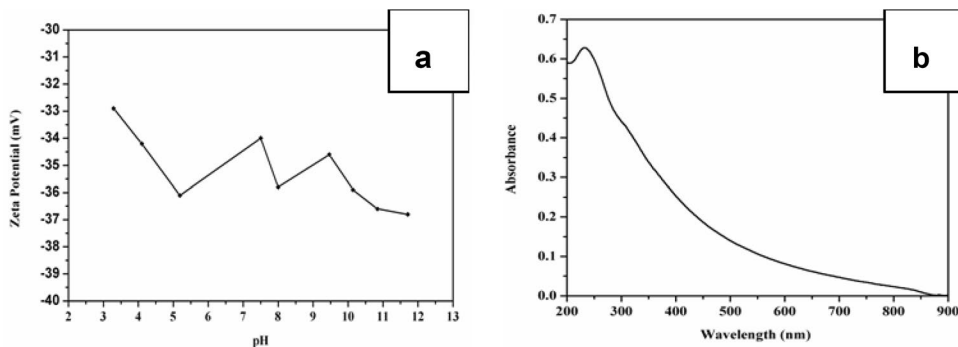
Fig. 3 XPS spectra of C 1s and O 1s and its de-convoluted profiles for **a, b** GO flakes produced by modified Hummers' method, **c, d** 316L SS substrates coated with GO suspension of pH 3.4 and **e, f** 316L SS substrates coated with GO suspension of pH 11

Fig. 4 a Zeta potential as a function of suspension pH and **b** UV–Vis spectrum of the GO suspension produced by modified Hummers' method

associated with chromophore units such as C=O, C=C, and C–O bonds linkage. The intensity of the π–π* plasmon peak could be correlated with the conjugation effects of chromophore concentration. The shoulder peak observed at ~300 nm corresponded to the n–π* plasmon transition (transitions of C=O bonds) in GO.

3.3 Characterization of GO-Coated 316L SS

Raman spectra recorded on the 316L SS substrates coated with GO suspensions under acidic pH (3.4) and alkaline pH (11) are shown in Fig. 5a. The spectra revealed a D band at 1343.07 cm^{-1} and a G band at 1605.8 cm^{-1} with I_D/I_G value of 1.007 and 1.004, respectively. The blue shift was observed in wave number of D and G bands for GO-coated substrates in comparison with GO flakes, which revealed the partial reduction of GO sheets and the higher values of I_D/I_G for GO-coated specimens compared to the value of 0.94 for GO flakes also depicted the same with restoration of sp^2 domain by the application of potential during EPD process as well as introduction of a low-defect density regime [19, 20] in GO-coated substrates. There was a broad second-order band (2D) observed for both the GO-coated substrates. The 2D band represented the second-order two-phonon process. Combined with the G band, 2D band is a Raman signature of graphitic sp^2 materials. 2D band exhibited a strong frequency dependency on the excitation laser energy. 2D band can be used to determine the number of layers of graphene. The broad 2D band represented oxidation of sp^2 carbon structure to sp^3 carbon structure and also indicated the presence of multilayer graphene structures in GO coatings. Generally, higher intensity is proportional to the mass, and hence the higher intense peak for GO-coated substrate with acidic GO suspension can support the dense deposition in this condition compared to the GO-coated

substrates with alkaline suspension. The ATR-FTIR spectra were taken to reveal the transmission band of different functional groups presented in electrophoretically deposited GO on 316L SS for different pH-varied GO suspensions. Figure 5b showed the ATR-FTIR transmission spectra of 316L SS substrates coated with GO suspension of pH 3.4 and pH 11 by EPD. Spectra revealed the absence of C-O stretching band in epoxy, C=O stretching band in carboxylic group, O–H stretching and bending bands in carboxylic acid group. The presence of C=C and C–H stretching bands was correlated with the partial reduction of GO during EPD [41]. Figure 3c and 3e shows XPS spectra of the C 1s core level obtained from the GO-coated 316L SS substrates using GO suspension of pH 3.4 and pH 11, respectively. The quantification result of de-convoluted C 1s spectrum showed the atomic percentage of sp^2 carbon in C=C regime for both the 316L SS substrates coated with GO suspension of pH 3.4 and pH 11 was 47%, which is higher than the value observed in GO flakes. The results confirmed the partial restoration of C=C skeleton upon reduction of oxygen functionalities by the applied electric field during EPD. Figure 3d and 3f shows XPS spectrum of the O 1s core level in 316L SS substrates coated with GO suspension of pH 3.4 and pH 11, respectively. The binding energy at 530.4 eV for both the 316L SS substrates coated with GO suspension of pH 3.4 and pH 11 revealed the oxygen is bonded to metal, which was not observed in GO flakes [42, 43]. The quantification result of de-convoluted O 1s spectrum showed the overall decrease in atomic percentage of oxygen of GO-coated substrates than GO flakes indicating the partial reduction.

AFM topography of 316L SS substrates coated with GO suspension under acidic and alkaline pH conditions is shown in Fig. 6a, d. The average roughness and root-mean-square (RMS) roughness are calculated and tabulated in Table 2. 316L SS substrates coated with GO in acidic pH showed
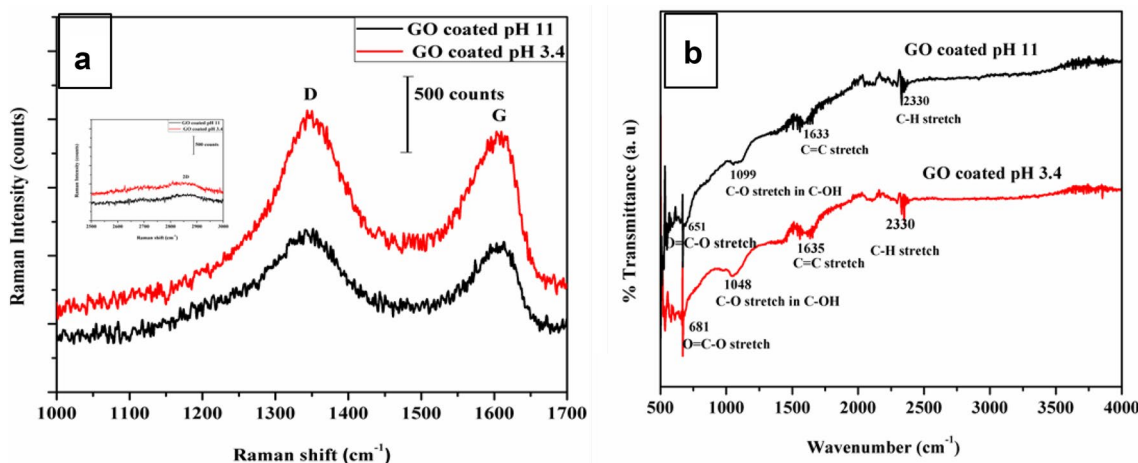

Fig. 5 **a** Raman and **b** ATR-IR spectra of 316L SS substrates coated with GO suspension of pH 3.4 (red) and pH 11 (black) (Color figure online)
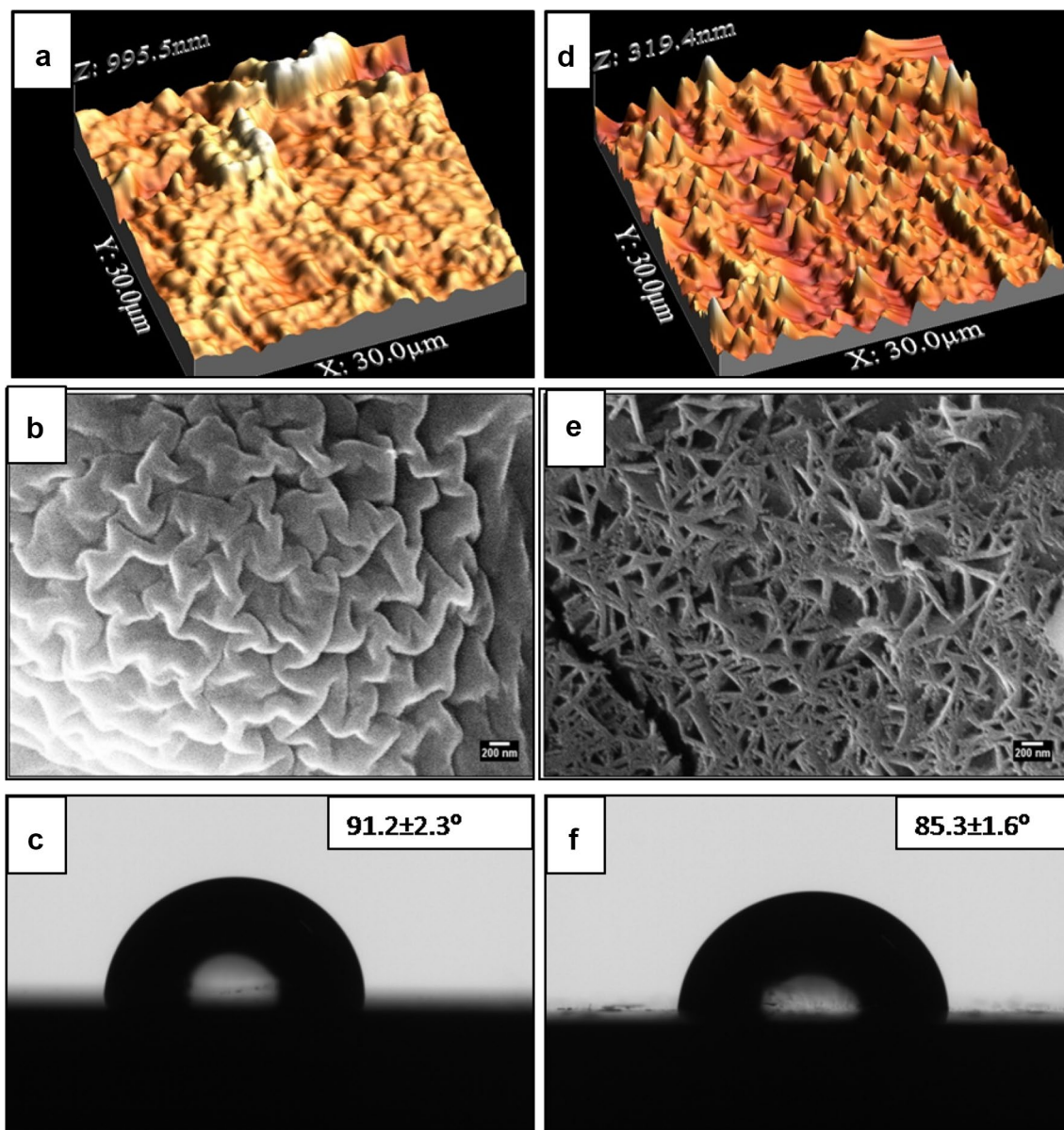
Fig. 6 AFM, FESEM, and WCA images of **a–c** 316L SS substrates coated with GO suspension of pH 3.4 and **d–f** 316L SS substrates coated with GO suspension of pH 11

Table 2 RMS roughness and average roughness values for GO flakes, 316L SS substrates coated with GO suspension of pH 3.4 and pH 11

Samples	Average roughness (R_a in nm)	RMS roughness (R_{rms} in nm)
GO flakes	155.7	200.0
316L SS substrates coated with GO suspension of pH 3.4	77.43	111.52
316L SS substrates coated with GO suspension of pH 11	29.19	37.86

higher RMS and average roughness in comparison with the 316L SS substrates coated with GO suspensions in pH 11. The FESEM images of GO-coated 316L SS samples deposited from acidic and alkaline GO suspensions, shown in Fig. 6b, e confirmed the dense agglomerated wrinkled morphology of GO coating obtained from acidic suspension and a interconnected branched network morphology of the GO coating produced from alkaline suspension [44]. Figure 6c, f shows the static WCA images of GO-coated 316L SS specimens. The contact angle values measured were $91.2 \pm 2.3°$ and $85.3 \pm 1.6°$ for the GO coatings from acidic and alkaline suspensions, respectively. Thus, the GO

coating on 316L SS substrate from acidic suspension exhibited hydrophobic characteristics in comparison with the GO coating from alkaline suspension. According to Cassie-Baxter model [45], heterogeneity of the coated surface acts as an effective block for the penetration of water molecules. The air pockets on the surface introduced by heterogeneity result in reduced water molecule penetration and thereby a higher WCA value. The higher RMS and average roughness values of the GO coating from acidic suspension could have contributed to higher heterogeneities, which in turn increased WCA values [46–49]. The WCA value characterizes their intrinsic wettability properties. The higher water contact angle value corresponds to low surface energy value [50]. So, it can be concluded that the GO coating on 316L SS substrate from acidic GO suspension has lower surface energy than GO coating on 316L SS substrate from alkaline GO suspension.

Thus, Raman, XPS, and ATR-FTIR spectra analysis confirmed the successful development of graphene coating on 316L SS substrate The increased value of I_D/I_G by Raman spectra analysis, partial restoration of C=C skeleton in the de-convoluted C 1 s XPS spectra analysis, and the presence of C–C and C–H stretching bands in ATR-FTIR spectra were also correlated with the partial reduction of GO during the deposition on 316L SS surface. Though there was no difference in the chemical composition of the coatings formed from the acidic and alkaline pH suspension, atomic force microscopy (AFM) and field emission scanning electron microscopy (FESEM) characterization showed difference in topography and morphology of the coatings. The structural model of GO shows hydrophobic property for its basal plane made up of polycyclic C=C domains and hydrophilic property for carboxylic group present along the edges. The negative charge is attributed to the ionization of carboxylic acid present along edges when these get hydrolyzed. The hydrophilic property of carboxylic acid can be varied by changing the pH from acid to alkaline. The different microstructures are likely due to the difference in hydrophilicity of GO under different pH values. 316L SS substrates coated by EPD in acidic suspension showed a dense wrinkled structure with higher average and RMS roughness. Under acidic conditions, GO sheets are more hydrophobic, which would force the sheets to squeeze each other when compressed, leading to dense microstructures. The dense agglomerated wrinkled morphology along with the presence of hydrophobic polycyclic C=C domain contributed to the higher hydrophobic nature of the coating. Under alkaline condition, GO sheets are more hydrophilic. Cote et al. mentioned about the water lubricating layer, which would allow them to form face-to-face adhering multilayer prior to deposition on the electrode finally upon deposition to form network structure. The acidic suspension had micron-sized particles and had a lesser negative zeta potential compared to the basic suspension with nanoparticles and more stable zeta potential value. As the particle size reduced and the distribution of particle size was narrow in the case of alkaline GO suspension, a GO coating with smoother lesser dense network morphology emerged. Under alkaline condition, GO sheets are more hydrophilic. Cote et al. [44] mentioned about the water lubricating layer, which would allow them to form face-to-face adhering multilayer prior to deposition on the electrode finally upon deposition to form network structure. Hasan et al. [19] mentioned the same network structure for alkaline GO coating on 316L SS. Thus, the present study showed that the microstructures of the GO coatings on 316L SS can be tuned by varying the pH of the GO suspension during EPD process.

4 Conclusion

Graphene oxide flakes were successfully synthesized by adopting modified Hummers' method, and the suspension of GO was used for the coating on 316L SS substrates by EPD under acidic and alkaline conditions. GO flakes and the pH-dependent microstructures of the GO-coated 316L SS coupons were characterized. The following conclusions were extracted from this study: Introduction of various oxygen functional groups in graphitic structure upon oxidation, the extent of disorder with a prominent D band, confirmed the GO formation. GO showed maximum weight loss due to pyrolysis of liable oxygen functional groups at 150 °C. The negative zeta potential value confirmed the stability of GO suspensions in both acidic and alkaline conditions. The increased value of I_D/I_G for GO-coated substrates than GO flakes showed the anodic reduction of GO during EPD. The C and O 1s spectra of GO flakes and both the GO-coated substrates revealed the partial reduction of GO during EPD. 316L SS substrates coated with GO in acidic pH showed higher RMS and average roughness value which leads to higher water contact angle in comparison with the 316L SS substrates coated with GO suspensions in pH 11. The morphology of GO-coated 316L SS samples deposited from acidic and alkaline GO suspensions confirmed the dense agglomerated wrinkled morphology of GO coating obtained from acidic suspension and smoother network morphology of the GO coating produced from alkaline suspension.

References

1. Johnson DW, Dobson BP, Coleman KS (2015) A manufacturing perspective on graphene dispersions. Curr Opin Colloid Interface Sci 20(5–6):367–382

2. Rao CE, Sood AE, Subrahmanyam KE, Govindaraj A (2009) Graphene: the new two-dimensional nanomaterial. Angew Chem Int Ed 48(42):7752–7777

3. Wang G, Wang B, Park J, Wang Y, Sun B, Yao J (2009) Highly efficient and large-scale synthesis of graphene by electrolytic exfoliation. Carbon 47(14):3242–3246

4. Choucair M, Thordarson P, Stride JA (2009) Gram-scale production of graphene based on solvothermal synthesis and sonication. Nat Nanotechnol 4(1):30–33

5. Wang G, Yang J, Park J, Gou X, Wang B, Liu H, Yao J (2008) Facile synthesis and characterization of graphene nanosheets. J Phys Chem C 112(22):8192–8195

6. Lerf A, He H, Forster M, Klinowski J (1998) Structure of graphite oxide revisited. J Phys Chem B 102(23):4477–4482

7. Konkena B, Vasudevan S (2012) Understanding aqueous dispersibility of graphene oxide and reduced graphene oxide through p K a measurements. J Phys Chem Lett 3(7):867–872

8. Lin CH, Yeh WT, Chan CH, Lin CC (2012) Influence of graphene oxide on metal-insulator-semiconductor tunneling diodes. Nanoscale Res Lett 7(1):343

9. Pei S, Cheng HM (2012) The reduction of graphene oxide. Carbon 50(9):3210–3228

10. Bykkam S, Rao KV, Chakra CS, Thunugunta T (2013) Synthesis and characterization of graphene oxide and its antimicrobial activity against klebseilla and staphylococus. Int J Adv Biotechnol Res 4(1):142–146

11. Liu S, Zeng TH, Hofmann M, Burcombe E, Wei J, Jiang R, Kong J, Chen Y (2011) Antibacterial activity of graphite, graphite oxide, graphene oxide, and reduced graphene oxide: membrane and oxidative stress. ACS Nano 5(9):6971–6980

12. Akhavan O, Ghaderi E (2010) Toxicity of graphene and graphene oxide nanowalls against bacteria. ACS Nano 4(10):5731–5736

13. Singh BP, Nayak S, Nanda KK, Jena BK, Bhattacharjee S, Besra L (2013) The production of a corrosion resistant graphene reinforced composite coating on copper by electrophoretic deposition. Carbon 61:47–56

14. Eda G, Fanchini G, Chhowalla M (2008) Large-area ultrathin films of reduced graphene oxide as a transparent and flexible electronic material. Nat Nanotechnol 3(5):270–274

15. Dumée LF, He L, Wang Z, Sheath P, Xiong J, Feng C, Tan MY, She F, Duke M, Gray S, Pacheco A (2015) Growth of nano-textured graphene coatings across highly porous stainless steel supports towards corrosion resistant coatings. Carbon 87:395–408

16. Bhaviripudi S, Jia X, Dresselhaus MS, Kong J (2010) Role of kinetic factors in chemical vapor deposition synthesis of uniform large area graphene using copper catalyst. Nano Lett 10(10):4128–4133

17. Zheng Q, Ip WH, Lin X, Yousefi N, Yeung KK, Li Z, Kim JK (2011) Transparent conductive films consisting of ultralarge graphene sheets produced by Langmuir–Blodgett assembly. ACS Nano 5(7):6039–6051

18. Cote LJ, Kim F, Huang J (2008) Langmuir–Blodgett assembly of graphite oxide single layers. J Am Chem Soc 131(3):1043–1049

19. Hasan SA, Rigueur JL, Harl RR, Krejci AJ, Gonzalo-Juan I, Rogers BR, Dickerson JH (2010) Transferable graphene oxide films with tunable microstructures. ACS Nano 4(12):7367–7372

20. An SJ, Zhu Y, Lee SH, Stoller MD, Emilsson T, Park S, Velamakanni A, An J, Ruoff RS (2010) Thin film fabrication and simultaneous anodic reduction of deposited graphene oxide platelets by electrophoretic deposition. J Phys Chem Lett 1(8):1259–1263

21. Chavez-Valdez A, Shaffer MS, Boccaccini AR (2012) Applications of graphene electrophoretic deposition: a review. J Phys Chem B 117(6):1502–1515

22. Diba M, Garcia-Gallastegui A, Taylor RN, Pishbin F, Ryan MP, Shaffer MS, Boccaccini AR (2014) Quantitative evaluation of electrophoretic deposition kinetics of graphene oxide. Carbon 67:656–661

23. Wang M, Duong LD, Oh JS, Mai NT, Kim S, Hong S, Hwang T, Lee Y, Nam JD (2014) Large-area, conductive and flexible reduced graphene oxide (RGO) membrane fabricated by electrophoretic deposition (EPD). ACS Appl Mater Interfaces 6(3):1747–1753

24. Park JH, Park JM (2014) Electrophoretic deposition of graphene oxide on mild carbon steel for anti-corrosion application. Surf Coat Technol 254:167–174

25. Hamaker HC (1940) Formation of a deposit by electrophoresis. Trans Faraday Soc 35:279–287

26. Eliaz N, Sridhar TM, Kamachi Mudali U, Raj B (2005) Electrochemical and electrophoretic deposition of hydroxyapatite for orthopaedic applications. Surf Eng 21(3):238–242

27. Ferguson SJ, Langhoff JD, Voelter K, Rechenberg BV, Scharnweber D, Bierbaum S, Schnabelrauch M, Kautz AR, Frauchiger VM, Mueller TL, van Lenthe GH (2008) Biomechanical comparison of different surface modifications for dental implants. Int J Oral Maxillofac Implants 23(6):1037–1046

28. Moravej M, Mantovani D (2011) Biodegradable metals for cardiovascular stent application: interests and new opportunities. Int J Mol Sci 12(7):4250–4270

29. Shankar AR, Mudali UK, Sole R, Khatak HS, Raj B (2008) Plasma-sprayed yttria-stabilized zirconia coatings on type 316L stainless steel for pyrochemical reprocessing plant. J Nucl Mater 372(2–3):226–232

30. Hummers WS Jr, Offeman RE (1958) Preparation of graphitic oxide. J Am Chem Soc 80(6):1339

31. Oh WC, Zhang FJ (2011) Preparation and characterization of graphene oxide reduced from a mild chemical method. Asian J Chem 23(2):875

32. Stobinski L, Lesiak B, Malolepszy A, Mazurkiewicz M, Mierzwa B, Zemek J, Jiricek P, Bieloshapka I (2014) Graphene oxide and reduced graphene oxide studied by the XRD, TEM and electron spectroscopy methods. J Electron Spectrosc Relat Phenom 195:145–154

33. Warren BE (1941) X-ray diffraction in random layer lattices. Phys Rev 59(9):693

34. Stankovich S, Dikin DA, Piner RD, Kohlhaas KA, Kleinhammes A, Jia Y, Wu Y, Nguyen ST, Ruoff RS (2007) Synthesis of graphene-based nanosheets via chemical reduction of exfoliated graphite oxide. Carbon 45(7):1558–1565

35. He H, Riedl T, Lerf A, Klinowski J (1996) Solid-state NMR studies of the structure of graphite oxide. J Phys Chem 100(51):19954–19958

36. Fu C, Zhao G, Zhang H, Li S (2013) Evaluation and characterization of reduced graphene oxide nanosheets as anode materials for lithium-ion batteries. Int J Electrochem 8:6269–6280

37. Ganguly A, Sharma S, Papakonstantinou P, Hamilton J (2011) Probing the thermal deoxygenation of graphene oxide using high-resolution in situ X-ray-based spectroscopies. J Phys Chem C 115(34):17009–17019

38. Oh YJ, Yoo JJ, Kim YI, Yoon JK, Yoon HN, Kim JH, Park SB (2014) Oxygen functional groups and electrochemical capacitive behavior of incompletely reduced graphene oxides as a thin-film electrode of supercapacitor. Electrochim Acta 116:118–128

39. Krishnamoorthy K, Veerapandian M, Yun K, Kim SJ (2013) The chemical and structural analysis of graphene oxide with different degrees of oxidation. Carbon 53:38–49

40. Lai Q, Zhu S, Luo X, Zou M, Huang S (2012) Ultraviolet-visible spectroscopy of graphene oxides. AIP Adv 2(3):032146
41. Mohammed Ali Al-Sammarraie A, Hasan Raheema M (2017) Electrodeposited reduced graphene oxide films on stainless steel, copper, and aluminum for corrosion protection enhancement. Int J Corrosion
42. Naumkin AV, Kraut-Vass A, Gaarenstroom SW, Cedric J. Powell NIST X-ray photoelectron spectroscopy database, NIST Standard Reference Database 20, Version 4.1
43. Cardenas L, MacLeod J, Lipton-Duffin J, Seifu DG, Popescu F, Siaj M, Mantovani D, Rosei F (2014) Reduced graphene oxide growth on 316L stainless steel for medical applications. Nanoscale 6(15):8664–8670
44. Cote LJ, Kim J, Zhang Z, Sun C, Huang J (2010) Tunable assembly of graphene oxide surfactant sheets: wrinkles, overlaps and impacts on thin film properties. Soft Matter 6(24):6096–6101
45. Cassie AB, Baxter S (1944) Wettability of porous surfaces. Trans Faraday Soc 40:546–551
46. Gao N, Yan Y (2009) Modeling superhydrophobic contact angles and wetting transition. J Bionic Eng 6(4):335–340
47. Vizhi ME, Vanithakumari SC, George RP, Vasantha S, Mudali UK (2016) Superhydrophobic coating on modified 9Cr–1Mo ferritic steel using perfluoro octyl triethoxy silane. Surf Eng 32(2):139–146
48. Förch R, Schönherr H, Jenkins AT (eds) (2009) Surface design: applications in bioscience and nanotechnology. Wiley, London
49. Vanithakumari SC, George RP, Mudali UK (2014) Influence of silanes on the wettability of anodized titanium. Appl Surf Sci 292:650–657
50. Cwikel D, Zhao Q, Liu C, Su X, Marmur A (2010) Comparing contact angle measurements and surface tension assessments of solid surfaces. Langmuir 26(19):15289–15294

Affiliations

Geetisubhra Jena[1,2] · S. C. Vanithakumari[1] · C. Thinaharan[1] · R. P. George[1] · U. Kamachi Mudali[2,3]

✉ R. P. George
rani@igcar.gov.in

1 Corrosion Science and Technology Division, Indira Gandhi Centre for Atomic Research, Kalpakkam 603 102, India
2 Homi Bhabha National Institute, Mumbai 400 094, India
3 Heavy Water Board, Mumbai 400 094, India